





# System Parameters Sensitivity Analysis of Ocean Thermal Energy Conversion

Rasgianti <sup>1</sup>, Ristiyanto Adiputra <sup>2\*</sup>, Ariyana D. Nugraha <sup>1</sup>, Ruly B. Sitanggang <sup>1</sup>,  
Wahyu W. Pandoe <sup>2</sup>, Aprijanto <sup>2</sup>, Takeshi Yasunaga <sup>3</sup>, Muhammad A. Santosa <sup>2</sup>

<sup>1</sup> Power Generation System Research Department, PT PLN (Persero) Research Institute, Jakarta Selatan, 12760, Indonesia.

<sup>2</sup> Research Center for Hydrodynamics Technology, National Research and Innovation Agency (BRIN), Surabaya 60112, Indonesia.

<sup>3</sup> Institute of Ocean Energy (IOES), Saga University, Saga, 840-8502, Japan.

## Abstract

Ocean Thermal Energy Conversion (OTEC) is a technology to harvest the solar energy stored in the ocean by utilizing the temperature difference between warm surface and cold deep seawater. Considering that the OTEC system works in a low-temperature range, the present paper assessed the technical resources comprehensively by acquiring in-situ thermocline data and conducting a sensitivity analysis of the system parameters. The in-situ temperature profile data were measured in the waters of North Bali, Indonesia. The temperature gradient data based on field measurements were then compared with the HYCOM consortium model. The data were then used as input in the OTEC power and efficiency estimation through a single-stage ranking cycle. The analysis was conducted by varying the type of working fluid, the performance of the heat exchanger, and the location to investigate how the system parameters influenced the power produced. Using an unusual combination of parameters made it difficult to analyze the resulting data multiple times. However, with reference-based analysis and the formulation of calculations, the sensitivity of each parameter could be assessed at both locations. As a result, the ammonia working fluid provided the highest net power output of the system but had the lowest efficiency of all working fluids. The heat exchanger performance in terms of net power and efficiency cannot be separated from the seawater mass flow requirement. This referred to the results where the heat exchanger with a temperature difference of 3°C before and after the seawater passed through the heat exchanger and produced the highest net power and efficiency. Additionally, the net power output reached its convergence level at a water depth of 400m for the Bungkulan site and 450m for Celukan Bawang, which was proportional to the thermocline tendency.

## Keywords:

Ocean Thermal Energy Conversion (OTEC);  
Temperature Profile;  
Single-Stage Rankine Cycle;  
Heat Exchanger;  
Net Power Output.

## Article History:

Received:	05	November	2023
Revised:	28	February	2024
Accepted:	11	March	2024
Published:	01	April	2024

## 1- Introduction

The application of renewable energy is a relevant energy source to support more environmentally friendly urban development [1]. Ocean Thermal Energy Conversion (OTEC) is a renewable energy source with underutilized potential that can be utilized without producing any greenhouse gas emissions or requiring fuel. The energy generated by OTEC power plants can replace fossil fuels [2], since OTEC plants produce electricity from solar energy by utilizing the temperature differential between the sun-warmed ocean surface and the cooler deep waters [3]. Despite their many advantages, OTEC power plants are not yet commercially viable.

\* **CONTACT:** [ristiyanto.adiputra@brin.go.id](mailto:ristiyanto.adiputra@brin.go.id)

**DOI:** <http://dx.doi.org/10.28991/ESJ-2024-08-02-04>

© 2024 by the authors. Licensee ESJ, Italy. This is an open access article under the terms and conditions of the Creative Commons Attribution (CC-BY) license (<https://creativecommons.org/licenses/by/4.0/>).

Marine conditions in Indonesia present substantial potential for the OTEC power plant development. Koto J, in 2016 [4], conducted research on the potential locations for OTEC power plants in Indonesia, including West Sumatra, North Sulawesi, Morotai Sea, and South Maluku. OTEC power plants in Indonesia can achieve an average cycle efficiency above 7%. Based on Sinuhaji's study [5], a power plant with a 125 kW capacity and a temperature difference of around 20.5°C in Bali, Indonesia, can generate a net power output of 69.4 kW with a cycle efficiency of 3.1%. Despite the significant potential of OTEC, there are currently no operational OTEC platforms in Indonesia.

Regarding the OTEC research in Indonesia, the baseline design and requirements for the OTEC floating platform were proposed by [6] in 2018. The baseline design was then applied to ship conversion from an oil tanker [7] as the plant ship for 100 MW-net OTEC to minimize capital expenditure by Monte Carlo simulation to yield the optimum size of the plant ship. The structural component of the seawater tank, subjected to dynamic pressure due to fluid movement inside the tank, was separately investigated to ensure the local strengthening system [8].

Adopting the general arrangement of a 100 MW-net OTEC plant ship proposed by [7], the Cold Water Pipe (CWP), installed to deliver seawater from a certain depth, was investigated, considering its dynamic stability due to the Internal Flow Effect (IFE) and its structural reliability under the bending load. The research on dynamic stability was initially conducted by investigating the dynamics component of CWP motion due to IFE [9] and then improved by solving the general equations in the frequency domain utilizing Power Series Expansion [10] and in the time domain by the Galerkin Method [11]. The analysis was then advanced by introducing finite element modeling (FEM) to assess the CWP responses in the frequency domain [12] and also in the time domain [13]. In the case of CWP structural reliability, non-linear assessments under bending loads [14] and parametric design following the finite element approach [15] were conducted.

In brief, the literature review on OTEC research and development in Indonesia highlights that the published works mainly focused on the theoretical potential assessment and the design of the supporting system for the OTEC plant ship. However, it is noteworthy that practical net power products play a crucial role in assessing OTEC implementation on an industrial scale. Thus, the OTEC net power calculation should be assessed comprehensively by ensuring the actual temperature data and considering the parameter sensitivity in the OTEC system. In broad terms, OTEC power plants generate a quantity of energy equivalent to the thermal energy extracted from seawater. The potential of these plants can be confirmed by comprehending the ocean heat content through analyzing the detailed temperature structure of the water column at a location of choice [16]. Thus, while a plethora of seawater column temperature databases exist, verifying the ocean heat content at the OTEC power plant site requires in situ measurements.

There are multiple approaches available to observing ocean heat content. One of the most frequently used techniques is the application of the conductivity-temperature-depth (CTD) instrument. The CTDs supplement current observations by progressively substituting discrete inverting thermometer measurements with uninterrupted temperature profiles. Modern CTDs are capable of precision reaching up to 0.001°C and 0.15% of full scale for pressure (1.5 m at 1000 m depth) and boast full digital capabilities [17]. Working fluid plays a critical role in OTEC systems [18]. The optimal working fluid must possess the appropriate thermophysical characteristics for its designated application and show chemical stability within the designated temperature range. The selection of the working fluid for OTEC systems must prioritize its thermal and cycle efficiency [19]. A closed-cycle OTEC system operates using a working fluid with a low boiling point, similar to the Rankine cycle. Pure working fluid enhances the power output, reduces the cycle's irreversible losses, and improves the effective temperature difference and working fluid temperature difference during both evaporation and condensation.

The thermal efficiency of OTEC systems is theoretically very low, necessitating a highly abundant heat source to compete with conventional power plants. It is imperative to ensure optimal performance of this component to realize maximum efficiency. Heat exchangers are utilized in the form of evaporators and condensers to transfer heat energy between seawater and the working fluid in OTEC systems [20]. The heat flow rate in this process is highly dependent on the performance of the heat exchanger.

Optimization of heat exchanger performance is critical to the maximization of net power output from OTEC power plants. The efficiency of the OTEC power plant and the flowrate requirements of seawater and working fluid to achieve the desired net power output are significantly affected by the performance of the heat exchanger [21]. In certain studies, the heat exchanger's efficacy is the foremost critical aspect scrutinized in OTEC systems [22]. The heat exchangers are examined and developed on OTEC to achieve higher efficiency.

Recent studies of the OTEC potential in Indonesia and the surrounding region have not used direct survey data for temperature. For example, Thirugnana et al. [23] conducted a study in Malaysia using data from the Japan Oceanographic Data Center (JODC). Similarly, the techno-economic study of Indonesia's OTEC potential by Langer et al. [24] utilized HYCOM data as the main temperature data at each location. On the other hand, most research on the potential of OTEC

power generation, especially in terms of net power calculation methods, has failed to include the energy required to operate the seawater pump. This is the case in the study by Samsuri et al. [25], which compared the efficiency of several working fluids but only calculated the efficiency of the working fluid pump. Similarly, research on the Rankine cycle OTEC performance by Thirugnana et al. [23] and Lee et al. [26] did not include seawater pumping. Even though cold seawater passes through pipes up to 400–1000 m in OTEC systems, the pressure drop that occurs will greatly affect the calculation results.

To improve the accuracy of net power and efficiency calculations in this study, the temperature data was based on the results of the researcher's survey at five points in two locations. Data collection was carried out directly using the bathymetric survey method at each point, leading to one of the main challenges in this study. In addition, calculations and comparisons were cross-checked between each main parameter to see the sensitivity of some of the main parameters. The variation in location is determined by the thermocline, seawater density, and survey distance from shore.

Currently, Indonesia has set a grand plan to reduce non-renewable electricity generation by 80% by 2045. This research aimed to demonstrate the potential of OTEC power plants as an alternative renewable energy power plant in Indonesia. In addition, cross-checked calculations were performed on three main parameters, working fluid type, heat exchanger performance, and different survey points, to determine the most appropriate parameters with the highest influence to be developed.

## 2- Methods

This study used a methodology similar to the flowchart shown in Figure 1. The research began with determining the survey point, followed by the survey data validation using data from the HYCOM consortium. The validated data were then analyzed through calculation methods to determine the net power output and also the efficiency of the cycle.

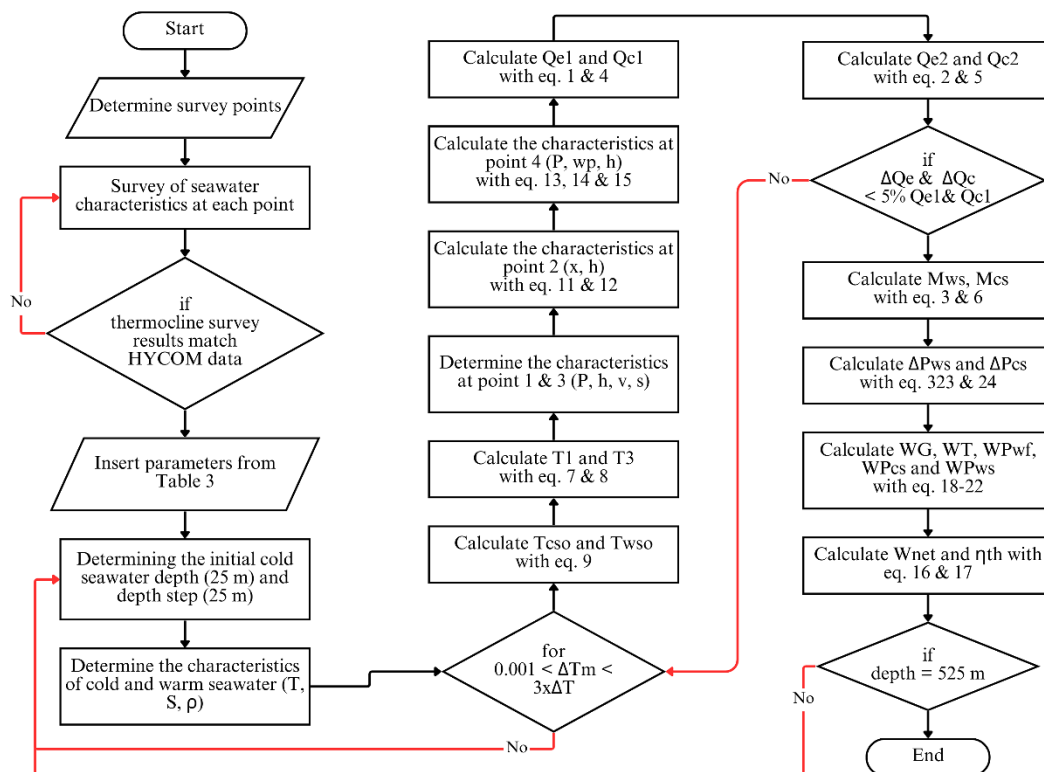
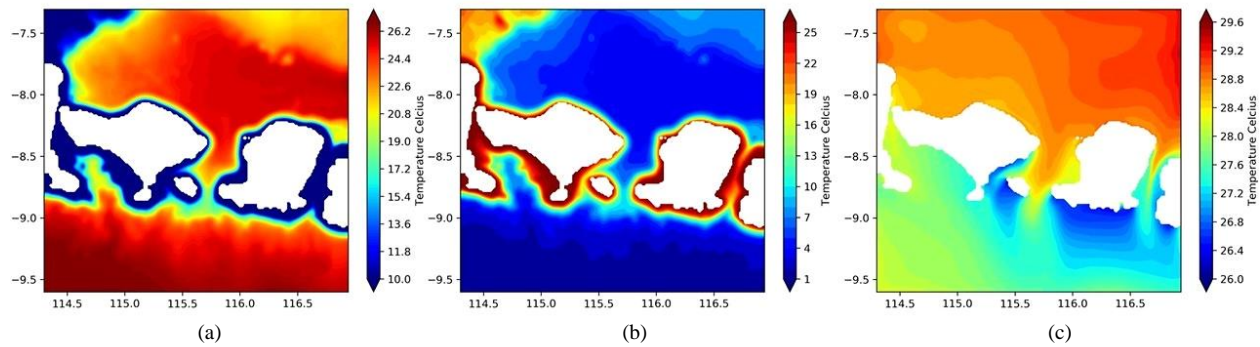


Figure 1. Research methodology flowchart

### 2-1- Temperature Profile Measurement

This research examined the sites in north Bali, Indonesia, as a case study. The temperature modeling in Figure 2 shows that the surface temperature of north Bali is about 28–29.5 °C, producing a temperature difference of nearly 22–25 °C with the seawater temperature at the bottom. This range of temperature is considerably excellent for OTEC implementation, where a temperature difference of 15–25 °C is required to achieve a thermal efficiency of about 3% [27]. In this study, the selected point only has a maximum depth of 600 m. This was based on the research by Syamsudin et al. [28], where in most areas in Indonesia, a sea temperature difference of more than 20 °C could be achieved at a depth of 500 m.



**Figure 2. Temperature at the North Bali: a) Surface temperature; b) Temperature at the bottom; c) Seawater temperature difference between surface and bottom**

The resource assessment of ocean thermal energy was performed by collecting temperature gradients in situ measurements. The properties of the water profile in the observation area were adopted along 3.78 nautical miles from the shoreline. Bathymetric surveys using single beam echosounder ODOM CV 100 emphasized the elevation of the bottom profile along predetermined track lines where an OTEC pilot plant could possibly be utilized and installed. Considering the location of latitude and longitude for seabed characterization during surveys, this research applied the GPS Garmin tool. The coordinates of the selected cast stations and the deployment location of specific CTDs (conductivity, temperature, and depth) are presented in Figure 3 and Table 1. Data collection was carried out at 5 station points in the North Bali Sea, including 2 sites in Bungkulan and 3 sites in Celukan Bawang.



**Figure 3. Cast location's maps from North Bali Sea**

The main instrument for temperature and depth data recording was the SBE (Sea-Bird Electronic) 19plus CTD, which can measure the conductivity of seawater at a sampling frequency of 4 Hz at a water depth of 600 m. Seawater salinity can be calculated using conductivity data based on the water's temperature and pressure. Depth can also be determined by calculating water density from temperature and salinity using absolute pressure measurements. The real-time data were obtained by the CTD internal unit on which the battery and storage chip were installed. The recorded data measurement was performed in September 2023 on board TOROMBALA 02. The CTD is equipped with a steel member to protect against impact from environmental forces. The Kevlar rope is connected to a steel member used to dip this instrument by an electric winch into the water column at each station.

**Table 1. CTD cast locations from North Bali Sea**

No.	Site	Depth (m)	Latitude (S)	Longitude (E)
<b>Bungkulan</b>				
1	SB-1	400	8° 2' 44.95"S	115° 9' 59.15"E
2	SB-2	600	8° 2' 10.10"S	115° 10' 2.64"E
<b>Celukan Bawang</b>				
1	SCB-1	300	8° 10' 39.47"S	114° 51' 3.92"E
2	SCB-2	400	8° 10' 15.20"S	114° 51' 3.10"E
3	SCB-3	600	8° 8' 2.83"S	114° 51' 3.49"E

The temperature gradient data obtained by in-situ measurements were verified with global oceanographic predictions from the HYCOM consortium based on hind cast for 30-day and 7-day forecasts. The formulas of cold and water pressure power, water pipe area, and turbine efficiency effects could substitute the gradient temperature differences obtained from on-site measurements. The OTEC system generated a net power estimation with data models. The location chosen for the OTEC system development could be determined from the results of this power calculation.

## 2-2- OTEC's Rankine Cycle calculation

The fundamental principle of OTEC systems is to utilize the surface heat of seawater to convert the working fluid into vapor. The resulting vapor subsequently drives a turbine that generates electrical energy. The condensation of vapor from the turbine is accomplished by exploiting the cold temperature of deep seawater. Depending on the cycle type, OTEC systems can be classified into three main categories, including closed, open, and hybrid cycles. A closed-cycle OTEC plant is employed as the subject of inquiry in this study.

Closed-cycle OTEC employs a closed system heat engine that operates with a working fluid. The system is based on Rankine Cycle, one of the most common thermodynamic cycles. The Rankine Cycle consists of four thermal processes, including isentropic compression, isentropic heating, isentropic expansion, and isobaric condensation, all of which occur within an idealized cycle [29]. The Rankine Cycle System is comprised of an evaporator, condenser, turbine, working fluid pump, generator, and connecting pipes between each component.

Figures 4 and 5 show the flow chart and conceptual temperature entropy (T-s) diagram of the Rankine Cycle, with each number at the position shown indicating each point of the working fluid state. The working fluid is delivered to the evaporator by the working fluid circulating pump (3  $\Rightarrow$  4), and heat transfer from the surface seawater to the working fluid occurs, producing saturated steam (4  $\Rightarrow$  1). The steam then expands to a lower pressure through the turbine and drives it (1  $\Rightarrow$  2). After the steam leaves the turbine, the working fluid enters the condenser, exchanges heat with cold seawater, and is condensed into a liquid to repeat the cycle (2  $\Rightarrow$  3). The working fluid is then returned to the evaporator (3  $\Rightarrow$  4).

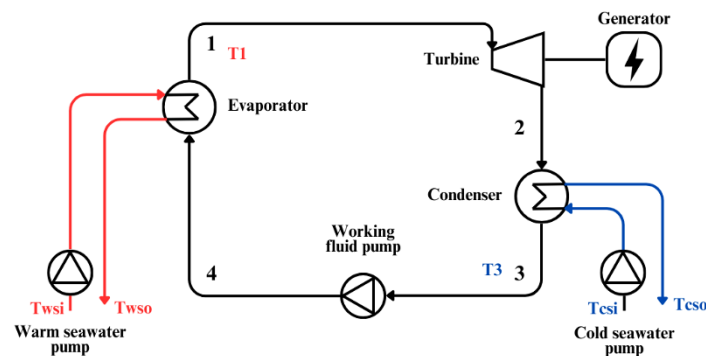


Figure 4. Rankine cycle

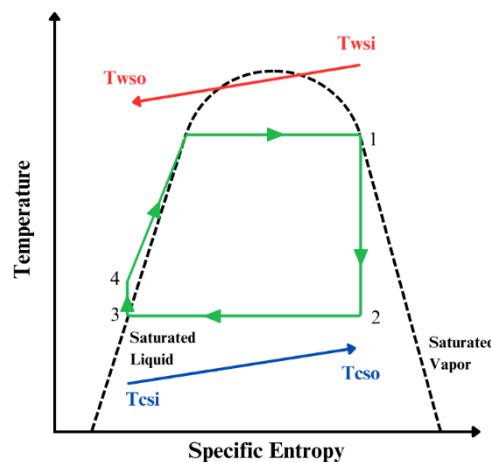


Figure 5. Specific Entropy-Temperature (T-s) of the Rankine cycle

The calculation of the net power output in the Rankine Cycle is based on the amount of power generated by the turbine ( $W_T$ ) minus the amount of power required to operate the working fluid pump ( $W_P$ ), warm seawater ( $W_{P,WS}$ ), and cold seawater ( $W_{P,CS}$ ). The Rankine Cycle performance analysis at each study site was performed using the following assumptions [30]:

- The working fluid is in a saturated vapor state at the outlet of the evaporator.
- The working fluid is in a saturated liquid state at the condenser outlet.
- The heat transfer part is negligible without the evaporator and at the condenser.
- The pressure loss of the working fluid is negligible at the connecting pipe, evaporator, and condenser.
- The potential energy of the working fluid is negligible.

The Rankine Cycle calculation is divided into two parts, namely the heat transfer system and the seawater pump system, which include warm and cold seawater pumps. The heat transfer system in the Rankine Cycle is calculated by dividing the system into two parts, the turbine and the working fluid pump. The turbine part occurs at points 1 and 2, the results of which are in the form of power generated by the turbine. The working fluid pump part occurs at points 3 and 4, with the results in the form of power required by the working fluid pump.

The Rankine Cycle system components themselves affect the performance of the Rankine Cycle heat transfer system. As shown in Equations 1 to 3 for the evaporator and 4-6 for the condenser, the heat flow rate in the Rankine Cycle is strongly influenced by the specifications of the components, including the performance of the pump, expressed in terms of the mass flow rate, in working fluid ( $m_{WF}$ ), warm seawater ( $m_{WS}$ ) or cold seawater ( $m_{CS}$ ), and the heat transfer area ( $A$ ) and heat transfer unit ( $U$ ) of the heat exchanger.

Heat flow rate in evaporator ( $Q_e$  ( $4 \gg 1$ ))

$$Q_e = m_{WF}(h_1 - h_4) \quad (1)$$

$$Q_e = UA(\Delta T m_e) \quad (2)$$

$$Q_e = m_{WS} c_{p,WS} (T_{wsi} - T_{wso}) \quad (3)$$

Heat flow rate in condenser ( $Q_c$  ( $2 \gg 3$ ))

$$Q_c = m_{WF}(h_2 - h_3) \quad (4)$$

$$Q_c = UA(\Delta T m_c) \quad (5)$$

$$Q_c = m_{CS} c_{p,CS} (T_{cso} - T_{csi}) \quad (6)$$

Where  $Q_{e,c}$  is Heat flow rate in the evaporator and condenser (kW),  $m_{WF}$  is Mass flow rate of working fluid ( $\text{m}^3/\text{kg}$ ),  $m_{CS,WS}$  is Mass flow rate of cold seawater and warm seawater ( $\text{m}^3/\text{kg}$ ),  $h$  is Working fluid enthalpy at each point (kJ/kg),  $c_{p,WS,CS}$  is Specific heat capacity (J/kg.K),  $\Delta T m_{e,c}$  is Temperature changes of the evaporator and condenser (K),  $T_{csi,o}$  is Cold seawater temperature at condenser inlet and outlet (K),  $T_{wsi,o}$  is Warm seawater temperature at evaporator inlet and outlet (K),  $U$  is Heat transfer unit of heat exchanger ( $\text{W}/\text{m}^2\text{K}$ ),  $A$  is Heat transfer area of heat exchanger ( $\text{m}^2$ )

The values of  $T_1$  and  $T_3$  are determined using Equations 7 and 8. In this report, the decrease and increase in seawater temperature after going through the evaporator and condenser are assumed to vary, where the value of cold seawater temperature increase is  $\Delta T_c = 1, 3$ , and  $5$ , and the value of warm seawater temperature decrease is determined by Equation 10. At points 1 and 3, the values of enthalpy ( $h$ ), entropy ( $s$ ), specific volume ( $v$ ), and pressure ( $P$ ) are known according to the thermodynamic table based on the type of working fluid and temperature ( $T_1$  and  $T_3$ ).

$$T_1 = \frac{e^{\left[\frac{T_{wsi}-T_{wso}}{\Delta T m_e}\right]} T_{wso} - T_{wsi}}{e^{\left[\frac{T_{wsi}-T_{wso}}{\Delta T m_e}\right]} - 1} \quad (7)$$

$$T_3 = \frac{e^{\left[\frac{T_{cso}-T_{csi}}{\Delta T m_c}\right]} T_{cso} - T_{csi}}{e^{\left[\frac{T_{cso}-T_{csi}}{\Delta T m_c}\right]} - 1} \quad (8)$$

$$T_{wso,cso} = T_{wsi,csi} - \Delta T_{e,c} \quad (9)$$

$$\Delta T_e = 1.2 \times \Delta T_c \quad (10)$$

where  $\Delta T_{e,c}$  is Seawater temperature change after getting out of evaporator and condenser (K).

Shortly after passing through the turbine (point 1  $\Rightarrow$  2), the working fluid remains in the saturated vapor phase as point 1 but has a temperature of point 3. The enthalpy at point 2 is closely related to the temperature at point 3 ( $T_3$ ). Therefore, the entropy value is calculated based on the thermodynamic table, assuming ( $T_2 = T_3$ ). Simultaneously, the enthalpy value at point 2 is determined using the following equation:

$$x_2 = (s_1 - s_2) / s_{fg,2} \quad (11)$$

$$h_2 = h_{f,2} + x_2 h_{fg,2} \quad (12)$$

where  $s$  is Working fluid's entropy at each point (kJ/mol),  $s_{fg}$  is Working fluid's difference entropy values between saturated liquid and vapor (kJ/mol),  $h_f$  is Working fluid's enthalpy values of saturated liquid (kJ/kg),  $h_g$  is Working fluid's difference enthalpy values between saturated liquid and vapor (kJ/kg).

Different from point 2, the calculation at point 4 does not necessarily correspond to the temperature at point 1 ( $T_1$ ). The enthalpy value at point 4 is determined using certain assumptions and equations.

$$P_4 = P_1 \quad (13)$$

$$wp_4 = -v(P_4 - P_3) \quad (14)$$

$$h_4 = h_3 - wp_4 \quad (15)$$

where  $P$  is Working fluid pressure at each point (kPa),  $v$  = Velocity of working fluid (m/s),  $wp$  is working fluid pump power at specific point (kW).

The net power output ( $\bar{W}$ ) and thermal efficiency ( $\eta_{th}$ ) of the OTEC system's cycle can be determined using the following equations:

$$\bar{W} = W_G - W_{P,WF} - W_{P,WS} - W_{P,CS} \quad (16)$$

$$\eta_{th} = \frac{\bar{W}}{Q_e} \quad (17)$$

where the power generated by the generator and the power required by the working fluid, warm seawater and cold seawater pump are calculated using the following formula:

$$W_G = W_T \eta_G \quad (18)$$

$$W_T = m_{WF}(h_1 - h_2)\eta_T \quad (19)$$

$$W_{P,WF} = m_{WF}(h_3 - h_4) / \eta_{P,WF} \eta_M \quad (20)$$

$$W_{P,WS} = m_{WS} \Delta P_{WS} / \rho_{WS} \eta_{P,SW} \quad (21)$$

$$W_{P,CS} = m_{CS} \Delta P_{CS} / \rho_{CS} \eta_{P,SW} \quad (22)$$

where  $\bar{W}$  is Net power output (kW),  $\eta_{th}$  is Thermal efficiency of OTEC system (%),  $W_G$  is Power generated by the generator (kW),  $W_T$  is Power generated by the turbine (kW),  $W_{P,WF}$  is Power needed to operationalize working fluid pump (kW),  $W_{P,WS,CS}$  is Power needed to operationalize warm and cold seawater pump (kW),  $\eta_G$  is Generator efficiency (%),  $\eta_T$  is Turbine efficiency (%),  $\eta_M$  is Motor efficiency (%),  $\eta_{P,WF}$  is Working fluid pump efficiency (%),  $\eta_{P,SW,CS}$  is Warm seawater and cold seawater pump efficiency (%),  $\rho_{WS,CS}$  is Density of warm seawater and cold seawater (kg/m<sup>3</sup>),  $\Delta P_{WS,CS}$  is pressure drops of warm and cold seawater (kPa).

The pressure drops of warm ( $\Delta P_{WS}$ ) and cold ( $\Delta P_{CS}$ ) seawater passing through a seawater pipe are determined using Equations 23 and 24, strongly influenced by the resistance to fluid flow ( $\gamma$ ). The length and size of the pipe affect the seawater pressure drop significantly, which in turn increases the power required by the warm and cold seawater pump.

$$\Delta P_{WS} = \gamma m_{WS}^k \quad (23)$$

$$\Delta P_{CS} = \gamma m_{CS}^k \quad (24)$$

$$\gamma = \frac{8\eta l_{CS,WS}}{\pi r^4} \quad (25)$$

where  $l_{CS,WS}$  is Length of warm seawater pipe and cold seawater pipe (m),  $\gamma$  is Resistance to fluid flow of seawater (Pa/m),  $r$  is Radius of seawater pipe (m),  $k$  is The water flow coefficient.



### 2-3-Heat Exchanger

In OTEC systems, the heat exchanger contributes significantly to exchanging heat from warm seawater to cold seawater. This component comes in two types: evaporators and condensers. The evaporator, specifically, is responsible for interacting with warm seawater, facilitating the exchange of heat from warm seawater to the working fluid. The heating process in the evaporator can be broken down into three stages, namely preheating, evaporation, and overheating [31]. The working fluid enters the evaporator as a saturated liquid and is heated to a saturated vapor state. The condenser function is nearly identical to that of the evaporator, differing only in the heat transfer between the working fluid and cold seawater. Upon exiting the condenser, the working fluid returns to a liquid state.

The amount of heat exchanged within the heat exchanger significantly affects the net power produced by the OTEC system. Furthermore, the performance of the heat exchanger greatly affects the OTEC power plant's efficiency and the necessary seawater and working fluid flow rates needed to attain the desired net power output [21]. The heat exchanger's performance will indirectly impact the cold water pipe's diameter, the seawater pump's size, and the overall OTEC platform size. The sensitivity analysis by Sinama et al. [32] demonstrated significant impacts of the heat exchanger on the OTEC cycle. The heat exchanger's performance assessment is critical to determining an OTEC power plant's net power output.

OTEC systems use several types of heat exchangers, with plate heat exchangers being one of the most studied [22]. Plate heat exchangers comprise a stack of plates, through which thermal energy is transferred from a relatively hot fluid to a cooler one. Each fluid flows on different sides of the plates. This report employs a plate heat exchanger with identical specifications between the evaporator and condenser to emphasize the impact of CWP length and working fluid type on the results. The heat exchanger utilized is a Titanium plate heat exchanger, which has a fixed heat transfer area and thermal conductivity value, with respective values at 30500 m<sup>2</sup> and 4.693 W/m<sup>2</sup>K [33].

In the Rankine Cycle, the change in seawater temperature after passing through the heat exchanger indicates heat exchanger performance. The greater the temperature change, the more efficient the heat exchanger [34]. In calculating the performance of the OTEC cycle, most researchers, such as Eldred et al. [21], Fontaine et al. [22], and Yeh et al. [35], use the seawater outlet temperature as a parameter. In this report, the pump specifications and seawater pipe size are investigated for their optimal values. Temperature change is used as an independent variable to find the optimal value of the pump and seawater pipe, considering the temperature changes ( $\Delta T$ ) of 1, 3, and 5 K.

### 2-4-Seawater Pipe

The power output of the OTEC power plant is determined by the difference in enthalpy between the working fluid after passing through the evaporator and condenser. This difference is influenced by the temperature contrast that results from the interaction of warm and cold seawater with the evaporator and condenser, respectively. Indirectly, the temperature difference between warm and cold seawater influences the amount of electrical power generated by the OTEC system. Unlike warm surface seawater, which is mostly determined by the sun, the cold deep seawater used in OTEC systems can vary depending on the depth of water taken.

One of the most important supporting components in OTEC power plants is the Cold Water Pipe (CWP) used to supply deep seawater to cool the condenser. The larger the OTEC power plant, the greater the seawater temperature difference required and thus, the longer the CWP required. In this report, the calculation is carried out with the assumption that the CWP length varies and correlates with the variation in cold seawater temperature. To see the variation of CWP length on net power output and cycle efficiency of OTEC plants, thermal gradients are used, along with thermocline data in two areas located in North Bali, including Celukan Bawang and Bungkulan.

OTEC systems require a minimum 20 K thermal gradient between surface and deep water to achieve maximum efficiency [36]. At both locations, a temperature differential of 20 K can be attained through the usage of cold seawater above 500 m. The thermocline is limited to a depth of 525 m to reduce the pressure drop of cold seawater through the CWP. At the Celukan Bawang site in North Bali, the distance between the power plant and the cold seawater intake is 6.7 km, while at the Bungkulan site it is 3 km.

The optimal value of the length requirements for the cold and warm seawater pipe diameters is examined in this research. The diameter of the seawater pipe is determined using Equations 26 and 27, where the diameter is heavily influenced by the required mass flow rate of both warm and cold seawater in the system and seawater velocity ( $v_{sw}$ ). In addition to the pipe diameter, the seawater velocity is also important in determining the seawater pressure drop. In this study,  $v_{sw}$  is used with a value of 2 m/s, which is obtained by reference to Herrera et al. [37]. The values of the two seawater mass flow rates are determined using Equations 3 and 6. Unlike warm seawater, cold seawater has its diameter multiplied by a constant of 2 to reduce the pressure drop of the cold seawater as it flows through the pipe. The warm seawater pipe inlet has a set length of 100 meters. The length of the cold seawater pipe inlet is determined by the distance between the power plant location and the cold seawater collection point at each survey location, using Equation 28.



$$d_{wwp} = \sqrt{4 \times m_{ws} / \rho_{ws,cs} \pi v_{sw}} \quad (26)$$

$$d_{cwp} = 2 \times \sqrt{4 \times m_{cs} / \rho_{ws,cs} \pi v_{sw}} \quad (27)$$

$$l_{cs} = \sqrt{di^2 + d^2} \quad (28)$$

where  $d_{wwp,cwp}$  is Diameter of warm seawater and cold seawater pipe (m),  $m_{ws,cs}$  is Mass flowrate requirements of warm seawater and cold seawater (kg/s),  $v_{sw}$  is Seawater velocity through the pipe (m/s),  $di$  is Distance from plant location to cold seawater collection point (m),  $d$  is Cold seawater intake depth (m),  $l_{cs}$  is Cold seawater pipe inlet length (m).

## 2-5- Working fluid

Aside from system characteristics, the working fluid impacts the efficiency of OTEC systems significantly. The selection of the working fluid in OTEC power plants greatly affects the feasibility and performance of the entire system. In maximizing the net power output of the OTEC system, several categories must be considered when determining the appropriate working fluid. These categories comprise [38]:

- The critical temperature exceeds the maximum temperature during the OTEC cycle, allowing evaporation of the working fluid, which in turn increases its specific heat significantly.
- The specific volume in both vapor and liquid states is relatively low, which affects the rate of heat transfer in the heat exchanger.
- High thermal conductivity of the liquid determines the heat transfer rates in the heat exchangers.
- Low liquid viscosity leads to a high heat transfer rate in the heat exchanger.
- High ratio of latent heat of vaporization ( $h_{fg}$ ) to specific volume ( $v_g$ ) under high vapor pressure conditions. Vapor conditions signify the heat transfer in the working fluid for each unit volume. Therefore, the greater the ratio of  $h_{fg}$  to specific volume, the greater the heat transfer.

The preferred working fluid for OTEC power plants is ammonia due to its ideal physical properties for OTEC cycles [2]. In a study conducted by Hung et al., various working fluids, including R11, R12, R152a, R500, R502, R113, R114, R123, C6H6, C7H8, or C8H10, were analyzed for OTEC cycles [39], indicating that higher cycle efficiency is achieved with working fluids that have higher latent heat values. Sun et al. conducted the analysis and optimization of the Rankine cycle, comparing ammonia and R134a as working fluids, indicating ammonia as the most practical working fluid to increase net power output [40].

It is essential to identify the optimal working fluid to optimize both the net power output and efficiency of the OTEC power plant cycle. This report utilizes five working fluids, namely R290, R600a, R152a, R134a, and Ammonia. The thermodynamic properties of each working fluid are provided in Table 2.

**Table 2. Thermodynamic properties of the working fluid used**

Properties	R290	R600a	R152a	R134a	Ammonia
Molecular weight (g/mol)	44.100	58.120	66.000	102.032	17.031
Boiling temperature (°C)	-42.10	-11.80	24.70	-26.30	-33.33
Critical temperature (°C)	96.70	134.98	113.50	101.21	132.41
Critical pressure (Bar)	42.50	36.60	45.00	405.93	113.57
Critical Density (kg/m <sup>3</sup> )	220.48	221.00	365	511.90	243.99
$v_g$ (m <sup>3</sup> /kg, @24°C)	0.04973	0.000126	0.059453	0.0343	0.14922
$h_{fg}$ (kJ/kg, @24°C)	337.490	330.010	280.570	178.700	1169.950
$s_{fg}$ (kJ/kg.K, @24°C)	1.1357	1.111	0.9442	0.601	3.937
ODP	0	0	0	0	0
GWP	3.0	4	124.0	1300	0
ASHRAE	A3	A1	A2	A1	A2L

In addition to the working fluids used in the system, the mass flow rate of the working fluid throughout the OTEC system is also an important factor influencing the performance of the OTEC system. As shown in equations. 1 and 4, the mass flow rate value becomes the main multiplier of the working fluid enthalpy difference to determine the system output power. In the Rankine Cycle, the mass flow rate at the inlet and outlet of each point is the same in the steady state [40-42]. This study uses a working fluid mass flow rate of 250 m/s. The mass flow rate value is used after trial and error and is intended to achieve a net power output value of at least 10 MW at one of the measurement points.

### 3- Parameter Configuration

In this research, the discussion focuses on the net power output, cycle efficiency, and seawater pipe diameter requirements, considering differences in location, working fluid, and heat exchanger performance. The difference in location is assumed through the difference in thermal gradient taken from the thermocline of the two study sites. Working fluid differences are investigated using thermodynamic property differences of the five working fluids (R290, R600a, R152a, R134a, and Ammonia). The difference in heat exchanger performance is assumed as a reduction and increase in seawater temperature after going through the evaporator and condenser.

MATLAB software is used to ensure the accuracy of the calculation results. The calculation program is based on the equations listed previously. The same program is used for all calculations to ensure consistent results. Several configuration parameters are used to provide a standardized approach to variable problems, including efficiency and component specifications. Of particular note are the primary components of the OTEC cycle, comprising the heat exchanger, turbine, and pump. The configuration parameters used are presented in Table 3.

**Table 3. Configuration of mass energy heat balance calculation parameters**

Parameters	Symbols	Value
Generator efficiency (%)	$\eta_G$	96
Turbine efficiency (%)	$\eta_T$	85
Working fluid pump efficiency (%)	$\eta_{P,WF}$	85
Seawater pump efficiency (%)	$\eta_{P,SW}$	85
Electric motor efficiency (%)	$\eta_M$	89
Thermal conductivity of heat exchanger (W/m <sup>2</sup> K)	$U$	4.693
Total heat transfer area of heat exchanger (m <sup>2</sup> )	$A$	30500
Mass flowrate of working fluid (kg/s)	$m_{WF}$	250
Seawater velocity through the pipe (m/s)	$v_{sw}$	2
Length of warm seawater inlet pipe (m)	$l_{WS}$	100
Warm seawater collection depth (m)		10
Maximum depth of cold seawater intake (m)		525
The water flow coefficient	$k$	2
Maximum heat transfer calculation error (%)	$Q_{error}$	5
Seawater temperature difference after going through the condenser	$\Delta T_c$	1, 3, 5

## 4- Results

### 4-1- Thermal and Density in Situ Measurement

The vertical temperature measurements at each location are targeted at water depths of 350 m and 550 m, except for one of the waters in Celukan Bawang (ST-1), which has a depth of 250 m. The water depth at the station sites was given a gap from the seabed with a CTD instrument lowering of 50 m. The results of deploying measurement equipment in the North Bali Seas provide a measured depth less than the target due to the currents that shift the horizontal position.

In this research, the temperature profile measured at the stations was the daily temperature distribution. The temperature gradient results were based on field measurements compared directly with the HYCOM consortium model. Retrieval of prediction model data from the HYCOM consortium was carried out on the website: <https://livingatlas.arcgis.com> for the same period as in-situ temperature measurements. The sea temperature model in the global prediction system used a resolution format from the HYCOM + NCODA global 1/12 analysis source with depth levels ranging from 0 m at the water surface to 5000 m. Direct comparisons were carried out to ensure the accuracy of field measurement data using CTD instrument.

In general, daily temperature values, the comparison results of in-situ measurements, and model estimations had good agreement in gradient temperature data trends in the North Bali Sea. As shown in Figure 6, the vertical temperature distribution from both the CTD and model could explain the gradual increase in temperature starting from a depth of 75 m to a depth of 150 m. The phenomenon of a significant gradient temperature at water depth is known as the thermocline layer. At water depths of 250 m to 550 m, there are no significant changes in sea temperature. Based on the measurement

results, the sea surface temperature was around 27.7 °C at Bungkulan and 28.5 °C at Celukan Bawang. According to the measurements, the temperature difference between the surface and cold water at a depth of 525 m was 21.2 °C at Bungkulan to 21.7 °C at Celukan Bawang. These results are consistent with the findings of Syamsudin et al. [28], who found that temperature differences exceeded 21°C at 500 m depth in some Indonesian waters, such as around the islands of Kalimantan and Sulawesi.

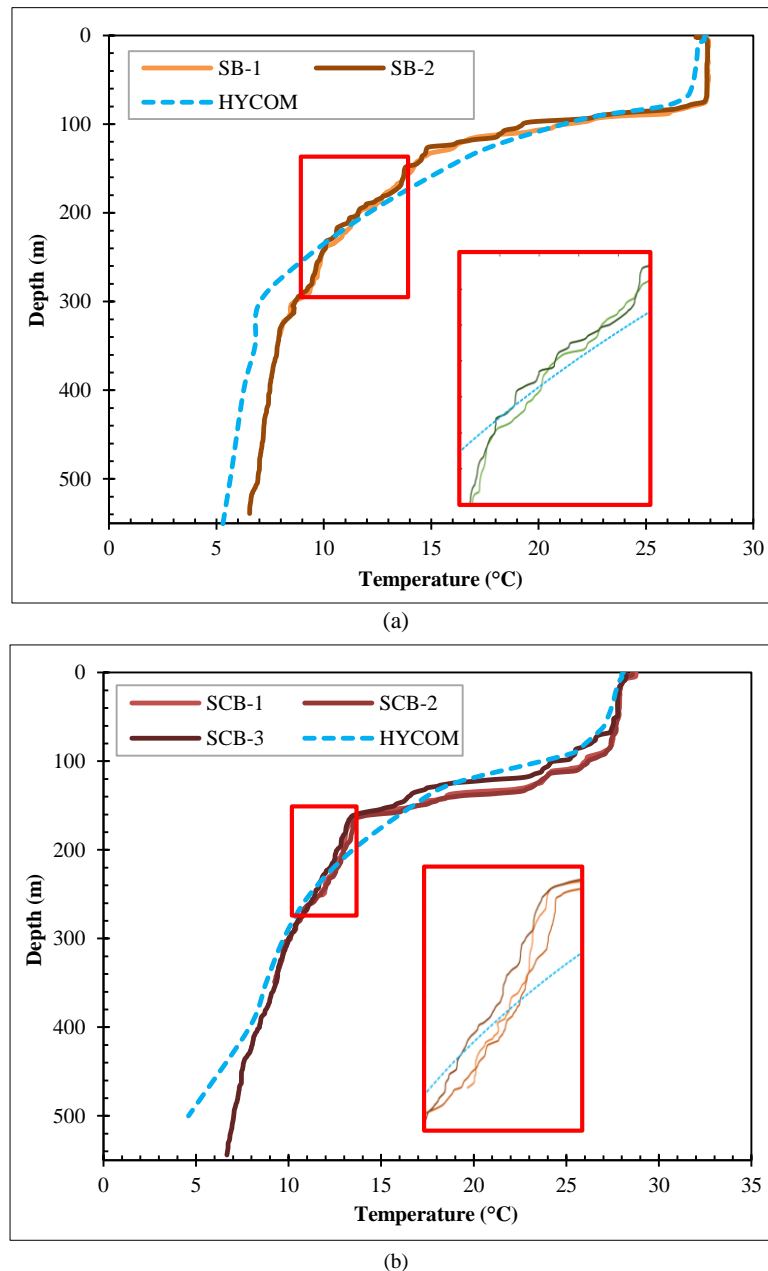


**Figure 6.** Thermocline at: (a) Bungkulan and (b) Celukan Bawang

#### 4-2- Working Fluid Selection Calculation Results

The OTEC power plant's net power output and cycle efficiency vary for each working fluid due to their distinct thermodynamic properties. To illustrate these differences, Figure 7 shows OTEC net power output at two Bali sites, Bungkulan (a) and Celukan Bawang (b), using a 3 K condenser temperature change ( $\Delta T_c = 3$ ). As highlighted in Figure 6, the net power output varies for all cycles with different working fluids at both locations. Based on the graphs from both locations, the cycle utilizing ammonia as the working fluid exhibits the highest net power output results when compared to the cycles employing other working fluids. In contrast, the cycle employing R134a demonstrates the lowest net power output. These results are consistent with the research conducted by Samsuri et al. [25] to find the most ideal working fluid for OTEC systems, including ammonia and R134a. Based on this research, ammonia working fluid produced the highest net power output among other pure working fluids, including R134a.

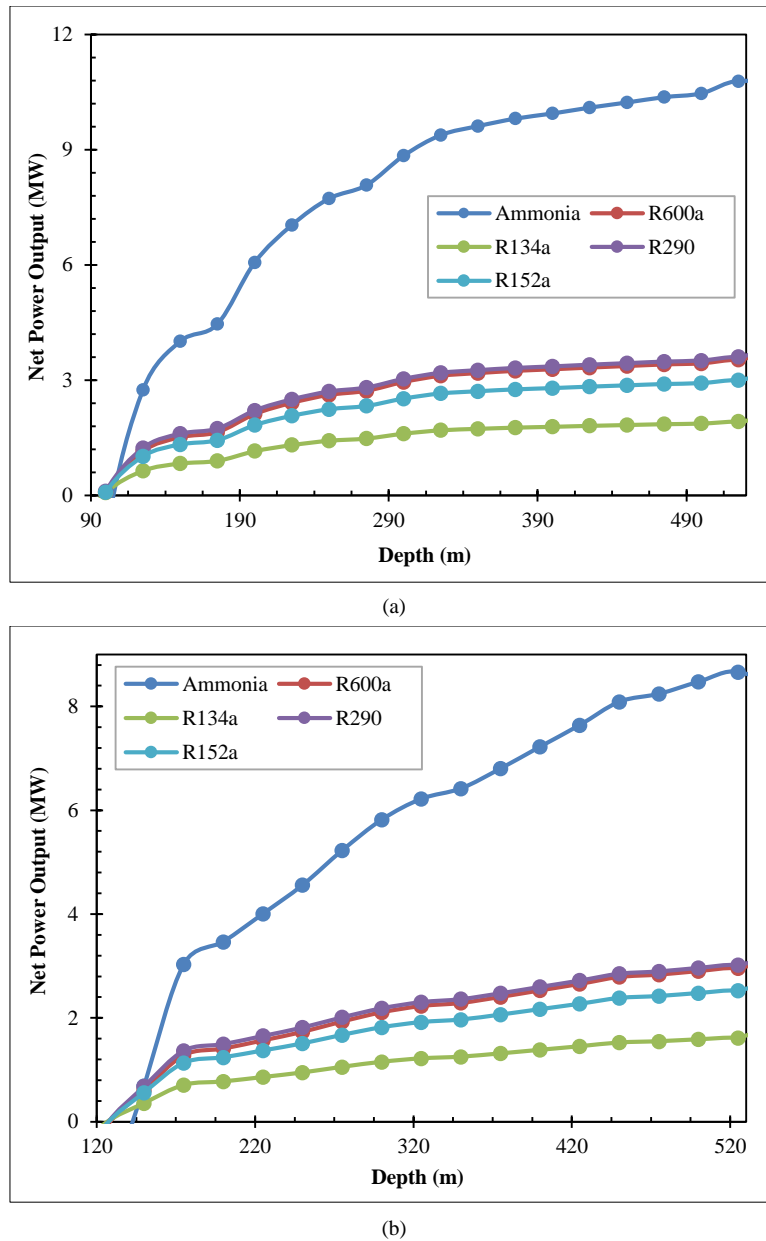


**Figure 7. Net power output for a  $\Delta T_c = 3$  K at: (a) Bungkulan dan (b) Celukan Bawang, Bali**

The net power output of the cycle using ammonia as the working fluid is significantly higher than other working fluids. The net power output of the ammonia cycle, using a cold seawater cycle of 525 m depth, is 10.78 MW at the Bungkulan site and 8.66 MW at Celukan Bawang. The power output of the cycle using R290 working fluid ranks second, with a net output difference of 7.18 MW at Bungkulan and 5.64 MW at Celukan Bawang locations, both with a cold seawater depth of 525 m.

In terms of the increasing trend, the increase in net power output converges after entering a cold seawater depth of 350 m at the Bungkulan location, while at the Celukan Bawang location, the increasing trend tends to converge but with a significant increase from the depth of cold seawater 200 m to 525 m. The maximum net power output at the Bungkulan site is significantly greater than that at the Celukan Bawang site.

The net power output results at both locations follow the working fluid enthalpy ( $h_{fg}$ ). The cycle sequence, based on the net power output results, is as follows: ammonia, R290, R600a, R152a, and R132a. This sequence coincides with the sequence of  $h_{fg}$ . The correlation between net power output and  $h_{fg}$  is also evident in the net power output cycle with R290 and R600a working fluids, which have similar values. This aligns with the difference in  $h_{fg}$  values between the two working fluids, which have a discrepancy of 7,480 kJ/kg.

Figure 8 displays the efficiency values for each cycle with  $\Delta T_c = 3$  and various working fluids at survey locations in Bungkulan, Bali (a), and Celukan Bawang, Bali (b). As in the net power output results, the efficiency trend between the working fluid at the Bungkulan and Celukan Bawang sites tends to be identical. The cycle with the highest efficiency is the cycle with working fluid R152a. At the Bungkulan location with cold seawater depth of 525 m, the efficiency of the

cycle with R152a working fluid is 3.27%, while at the Celukan Bawang location, at the same cold seawater depth and cycle, the cycle efficiency reaches 2.75%. Meanwhile, the cycle with ammonia working fluid has the lowest efficiency, where the cycle efficiency with ammonia working fluid is only 2.91% at the Bungkulan location and 2.34% at the Celukan Bawang location with cold seawater depth of 525m.

The efficiency of the four cycles using R134a, R290, R600a, and R152a as working fluids seems similar. The same value was observed at both survey locations. From the evaluation of the standard deviation at each depth of cold seawater for the three cycles, the average standard deviation at the Bungkulan site is only 0.0269, while the standard deviation at each depth of cold seawater at the Celukan Bawang location is only 0.0270

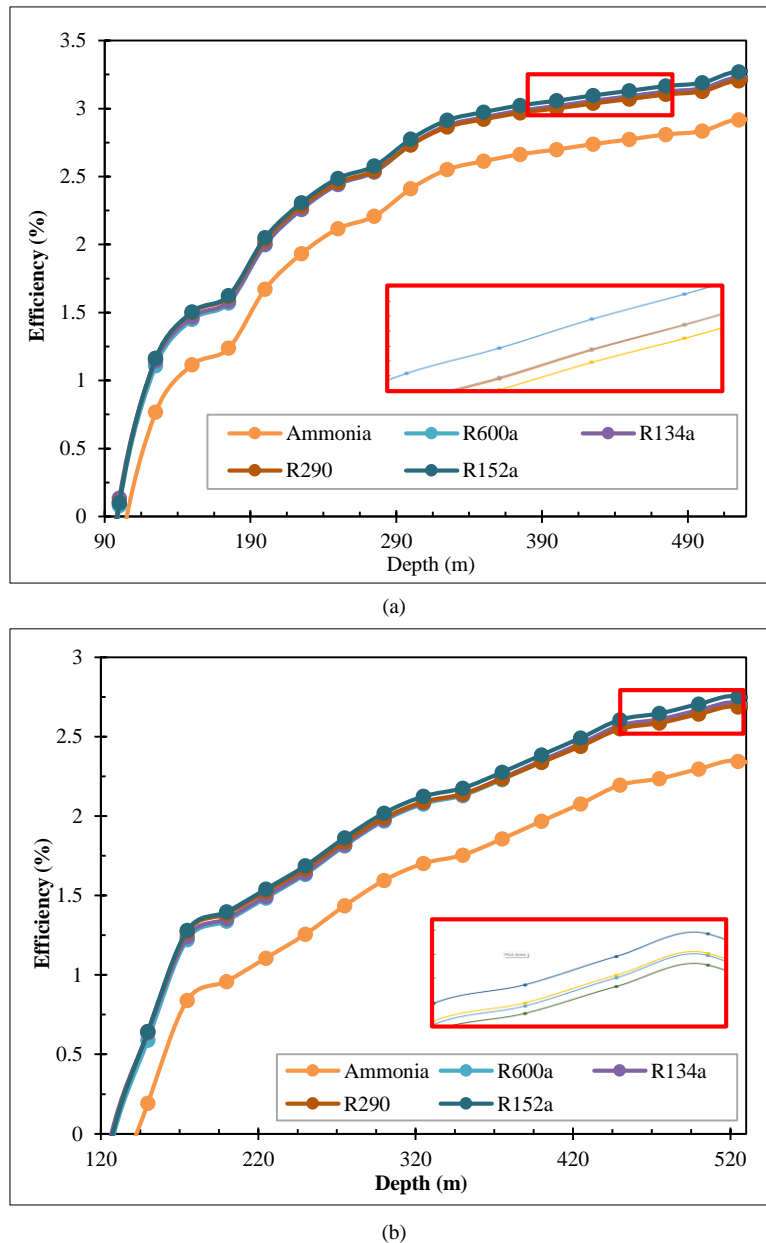


**Figure 8.** Cycle efficiency for a  $\Delta T_c = 3$  cycle at: (a) Bungkulan dan (b) Celukan Bawang, Bali

The efficiency trend in each cycle is inversely proportional to the net power trend. The cycle efficiency results are also inversely proportional to research conducted by Samsuri et al. [25], in contrast to the similarity in net power output. This difference in results occurs because Samsuri et al. [25] used the same seawater mass flow rate between each working fluid in their research, whereas in this study, the mass flow rate between each working fluid is differentiated according to the mass flow rate required to achieve the heat exchanger performance. Thus, the required pump power is different for each working fluid, with the increase in pump power affecting the efficiency of the OTEC cycle negatively. According to Figure 9, at both locations, the cycle with ammonia as the working fluid requires significantly more pump power than the other cycles. The power consumption of the cycles utilizing ammonia and R290 as working fluids differs by 1.38 MW at the Bungkulan site and 2.65 MW at the Celukan Bawang site.

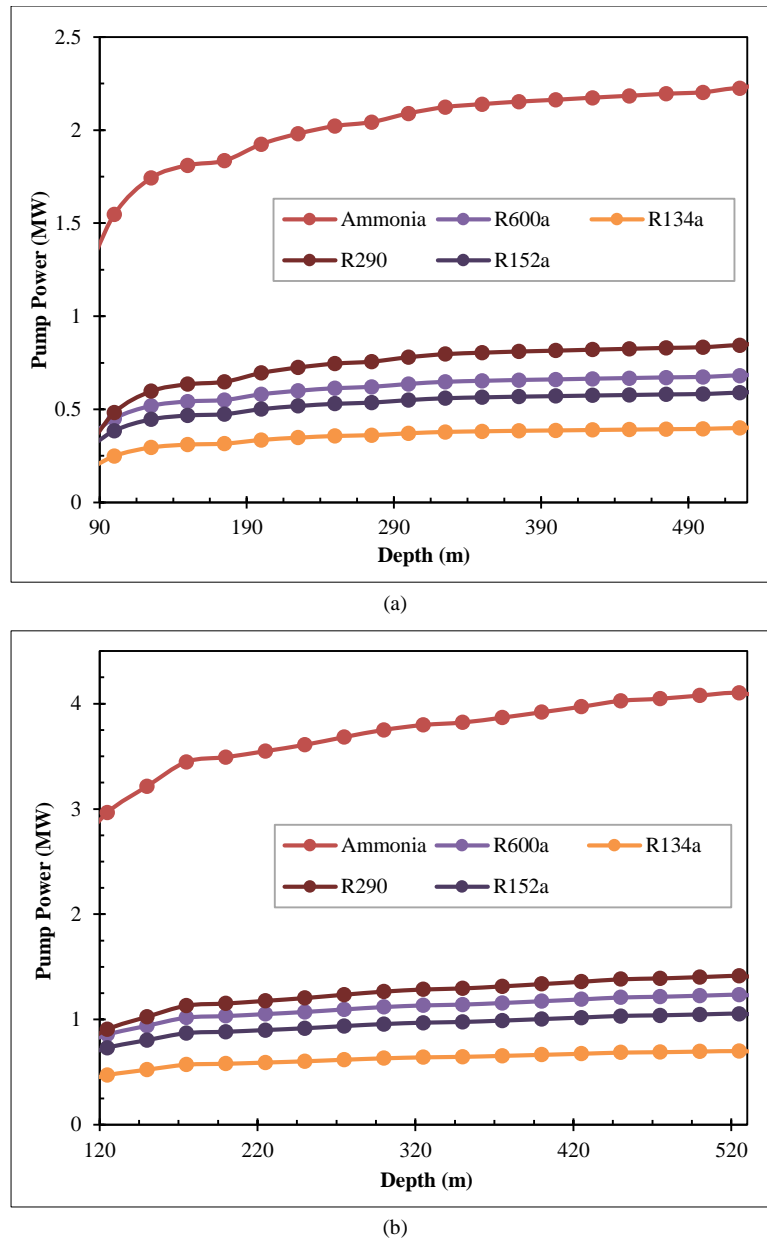


**Figure 9.** Total pump power requirements for a  $\Delta T_c = 3$  cycle at: (a) Bungkulan dan (b) Celukan Bawang, Bali

At the Celukan Bawang site, both the net power output and resulting efficiency are lower than at the Bungkulan site due to higher pump power requirements. This is caused by the greater distance between the cold seawater collection location and the shoreline at Celukan Bawang compared to Bungkulan. The cold seawater pressure experiences a significant reduction as it passes through the CWP, thereby increasing the power requirement of the cold seawater pump. At the Bungkulan location, the cold seawater pump accounts for 65% of the total pump power requirement, whereas it accounts for 80% at the Celukan Bawang location.

#### 4-3- Heat Exchanger Performance Selection Calculation Results

The study considers the heat exchanger performance based on seawater temperature decrease and increase after passing through the evaporator and condenser. Equations 1-3 and 4-6 for the evaporator and condenser, respectively, indicate that the heat exchanger performance greatly depends on the seawater temperature, heat exchanger area, thermal conductivity, and mass flow rate.

Table 4 shows that as heat exchanger performance improves (with a smaller  $\Delta T_c$  value), more pump power is needed at each location. This increase in pump power is required for all working fluid types and is the highest for the cycle using ammonia as the working fluid, which also generates the highest net power output. The difference in location, especially the distance between the cold seawater collection point and the coastline, affects the power pump requirements significantly. The Celukan Bawang site, in a cycle with  $\Delta T_c = 1$  and ammonia as the working fluid, requires 5.61 MW



more pump power than the Bungkulan site. In all variations of  $\Delta T_c$  and working fluid, the Celukan Bawang site exhibits an average pump power requirement that is 180% higher compared to the Bungkulan site. This marked contrast in pump power requirements results in the Celukan Bawang site generating a lower net power output and efficiency. The seawater pump power requirement is closely related to the seawater mass flowrate as shown in Table 5

**Table 4. Pump power required for each  $\Delta T_c$  parameters, working fluid and each location using 525m cold seawater**

	Working Fluid	Bungkulan			Celukan Bawang		
		1	3	5	1	3	5
Pump Power (MW)	Ammonia	6.292	2.225	1.364	11.905	4.102	2.497
	R600a	1.909	0.681	0.413	3.580	1.234	0.743
	R134a	1.078	0.399	0.245	1.987	0.701	0.425
	R290	2.144	0.845	0.527	3.858	1.414	0.867
	R152a	1.618	0.589	0.361	3.012	1.054	0.639

**Table 5. Mass flowrate for each  $\Delta T_c$  parameters, working fluid and each location using 525m cold seawater**

Working Fluid		Bungkulan			Celukan Bawang		
		1	3	5	1	3	5
Warm Seawater							
Mass flowrate (kg/s)	Ammonia	77292.96	25619.14	15265.43	77211.11	25593.78	15257.34
	R600a	23159.88	7573.98	4447.40	23141.83	7569.73	4445.09
	R134a	12624.63	4129.67	2428.16	12613.78	4126.43	2426.14
	R290	23787.26	7792.99	4584.10	23761.64	7786.14	4580.28
	R152a	19351.31	6357.98	3754.61	19335.18	6353.57	3752.04
Cold Seawater							
Mass flowrate (kg/s)	Ammonia	85133.08	28487.17	17172.89	85122.43	28481.81	17165.61
	R600a	25333.39	8387.64	4992.79	25320.59	8384.28	4990.95
	R134a	13795.55	4572.36	2727.00	13785.61	4569.15	2725.04
	R290	26011.17	8627.30	5145.53	25990.97	8620.77	5141.70
	R152a	21143.78	7036.46	4213.97	21131.87	7032.55	4211.57

Table 5 illustrates a considerable contrast in mass flowrate requirement between each parameter of  $\Delta T_c$ , particularly between cycles with  $\Delta T_c$  values of 1 and 3. This discrepancy is observed in all fluid variations at both locations. In both the Bungkulan and Celukan Bawang locations, and across all working fluid variations, the cycle with a temperature difference of  $\Delta T_c = 1$  reveals an average mass flowrate that is three times (300%) greater than the cycle with a temperature difference of  $\Delta T_c = 3$ . Similarly, the cycle with a temperature difference of  $\Delta T_c = 3$  has an average mass flowrate that is 1.6 times (160%) greater than the cycle with a temperature difference of  $\Delta T_c = 5$ . In addition to heat exchanger performance, the choice of working fluid also impacts the mass flow rate of seawater. Ammonia-based cycles demand a higher seawater mass flowrate compared to other working fluids. This indicates that cycles operating with ammonia require higher seawater mass flowrates at both locations and different  $\Delta T_c$  variations. This condition is consistent with the results of the net power output of the ammonia cycle, which has the highest value among cycles with other working fluids.

Figure 10 displays the net power output and cycle efficiency for each cycle, with varying seawater temperatures as the calculation parameters and ammonia as the working fluid. As shown in Figure 10a, the net power output for each cycle with variations in temperature changes after going through the condenser ( $\Delta T_c = 1, 3$ , dan 5) has a different trend between each location, attributed to the difference in pump power requirements. However, the cycle with  $\Delta T_c = 3$  has the highest net power output at both Bungkulan and Celukan Bawang sites. At the Bungkulan site, with cold seawater of 525 m depth, the net power output reaches 10.78 MW, while the net power output is 8.66 MW at the Celukan Bawang location using the same cycle parameters. On the other hand, the lowest net power output trend occurs in the cycle with  $\Delta T_c = 5$  for the Bungkulan site and the cycle with  $\Delta T_c = 1$  for the Celukan Bawang site. Despite the lowest net power output at its site, the cycle with  $\Delta T_c = 5$  at the Bungkulan site, almost always has a higher net power output than the cycle with  $\Delta T_c = 3$  at the Celukan Bawang site.

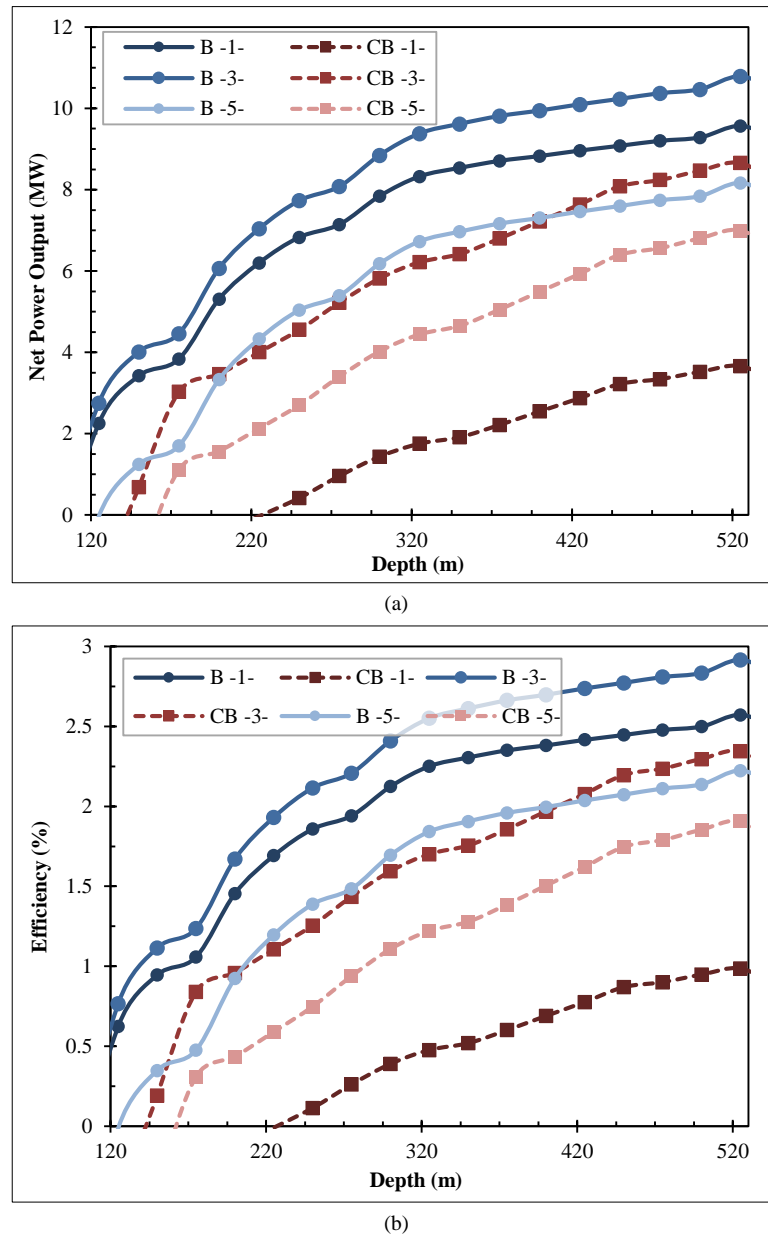


**Figure 10.** Net power output (a) and cycle efficiency (b) of cycles with ammonia working fluid with different heat exchanger performance at both survey sites (B=Bungkulan; CB=Celukan Bawang)

On the other hand, as shown in Figure 10b, the cycle efficiency with the variations of  $\Delta T_c = 1, 3$ , and 5, has the same trend as the net power output. The same trend occurs at all locations and all parameters of  $\Delta T_c$ , indicating that heat exchanger performance has the same influence on the net power output and cycle efficiency. The maximum efficiency at both locations is achieved in the cycle with  $\Delta T_c = 3$  and cold seawater depth of 525 m. At the Bungkulan site, the maximum cycle efficiency reached 2.92%, while it reached 2.34% at the Celukan Bawang site.

The results of both net power and efficiency are not completely consistent with the results of Yang & Yeh [42], where the lower the condensing temperature and the higher the evaporating temperature (the smaller  $\Delta T_{c,e}$ ), the higher the net power and cycle efficiency, attributed to the difference in seawater mass flow parameters. In their method, Yang & Yeh [42] used the seawater mass flowrate as a fixed parameter, so the pump power requirement is the same for each increase in  $\Delta T_{c,e}$ . However, in this study, the smaller the  $\Delta T_{c,e}$ , the larger the seawater mass flow requirement, which increases the seawater pump power requirement and causes the increase in  $\Delta T_{c,e}$  not to be fully negatively correlated with the net power and cycle efficiency. However, consistent with the results of Yang & Yeh [42], the cycle with the largest  $\Delta T_{c,e}$  ( $\Delta T_c = 5$ ) resulted in the lowest net power output and efficiency.

#### 4-4- Calculation Results of Sea Water Pipe Dimension

The seawater pipe diameter requirement is determined by Equations 26 and 27 and heavily impacted by the mass flowrate in each cycle. As shown in Table 6, the cold seawater pipe diameter is significantly larger than the warm seawater pipe diameter. This is consistent with Equation 27 which has a constant of 2. Table 6 shows that changes in

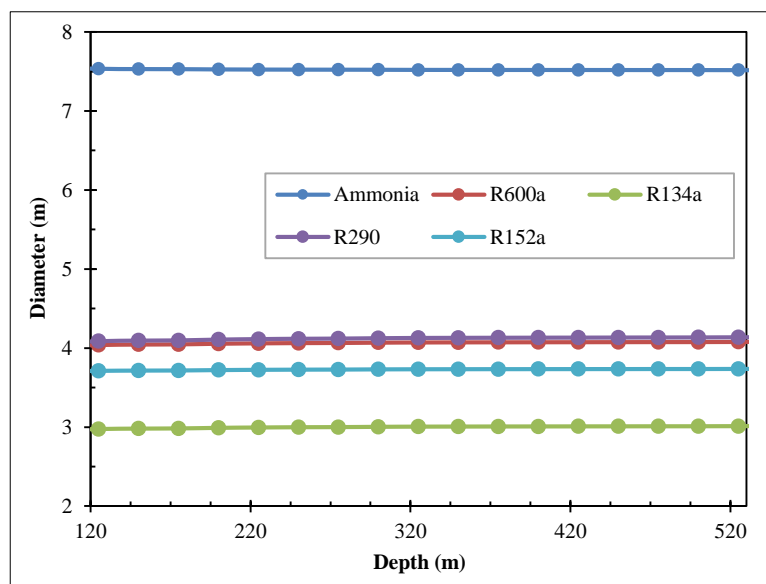
location do not affect the diameter of the seawater pipe significantly because according to equations 26 and 27, the diameter of the seawater pipe is determined by the mass flow rate rather than pipe length. In cold seawater pipes, the average diameter difference between Bungkulan and Celukan Bawang locations is only 0.0011 m in all parameters. Similarly, in warm seawater, the average diameter difference is only 0.0010 m, indicating that doubling the diameter as in equation 27 does not change the pipe diameter difference between each location.

**Table 6. Diameter of warm seawater pipe with cold seawater depth of 525 m**

Working Fluid	Bungkulan			Celukan Bawang		
	1	3	5	1	3	5
<b>Warm Seawater Pipe</b>						
Ammonia	6.208	3.574	2.759	6.205	3.572	2.758
R600a	3.398	1.943	1.489	3.397	1.943	1.489
R134a	2.509	1.435	1.100	2.508	1.434	1.100
R290	3.444	1.971	1.512	3.442	1.970	1.511
R152a	3.106	1.780	1.368	3.105	1.780	1.368
<b>Cold Seawater Pipe</b>						
Ammonia	12.994	7.517	5.836	12.994	7.516	5.835
R600a	7.089	4.079	3.147	7.087	4.078	3.146
R134a	5.231	3.011	2.326	5.229	3.010	2.325
R290	7.183	4.137	3.195	7.180	4.135	3.194
R152a	6.476	3.736	2.891	6.474	3.735	2.890

Concerning the heat exchanger performance in terms of temperature change after going through the condenser ( $\Delta T_c$ ), the diameter difference between cycles with  $\Delta T_c = 1$  and  $\Delta T_c = 3$  is quite significant. For example, in the cycle with ammonia working fluid, the diameter of the cold seawater pipe has a difference of 5.478 m at both locations. However, the diameter difference between the two locations in cycles  $\Delta T_c = 3$  and  $\Delta T_c = 5$  using ammonia working fluid is 1.681 m at both locations. These conditions occur due to the high seawater mass flow rate required to achieve heat exchanger performance that can realize  $\Delta T_c = 1$  compared to the other two variations.

On the other hand, the difference in diameter between each cycle with different working fluids corresponds to the difference in the net power output produced. In both warm and cold seawater pipes, the cycle with ammonia working fluid has the largest diameter, while the cycle with R134a working fluid has the smallest diameter. This shows that the type of working fluid is closely related to the seawater mass flow requirement to achieve the heat exchanger performance according to the given variation. According to equations 26 and 27, the mass flow rate value affects the diameter requirement of the seawater pipe. However, as depicted in Figure 11, in contrast to the possibility of a zero (0) net power output, the cold seawater pipe maintains nearly a uniform diameter across all depths.



(a)

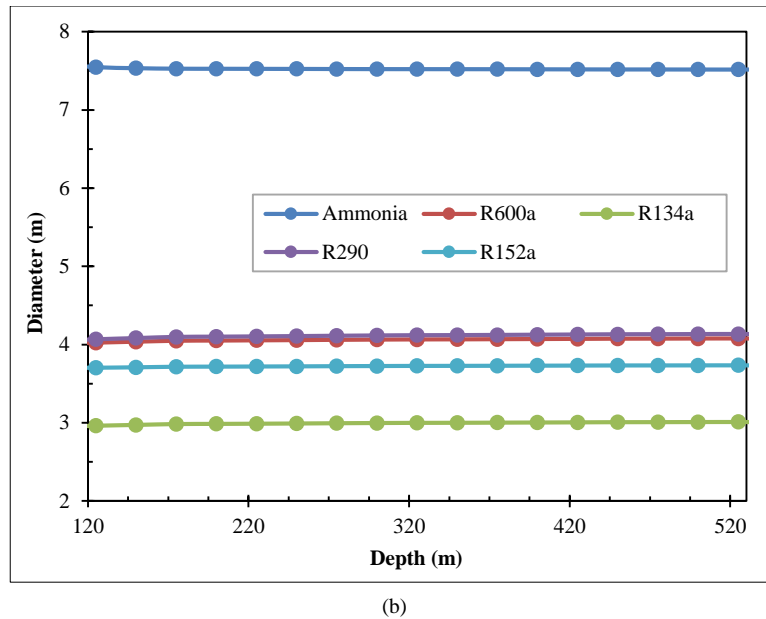


**Figure 11. Diameter of cold seawater pipe in cycle with  $\Delta T_c = 3$  at location (a) Bungkulan and (b) Celukan Bawang, North Bali**

As seen in Figure 11, the diameter of the cold seawater pipe in the  $\Delta T_c = 3$  cycle remains consistent at both the Bungkulan and Celukan Bawang locations. Not only is the trend consistent, but the diameter of the cold seawater pipe is also nearly identical at every depth of cold seawater. Across all depths and working fluids, there is little to no variation in the diameter of the cold seawater. The standard deviation for each cycle with varying working fluids is 0.0268 m at Bungkulan and 0.0265 m at Celukan Bawang. This result is consistent with Table 6, where differences in location have little effect on seawater mass flow requirements and seawater pipe diameters. It is also noteworthy that the depth or temperature of the cold seawater has almost no effect on the cold seawater pipe diameter requirements.

## 5- Conclusions

The present research estimated the practical net power output and efficiency of the OTEC system by conducting a site survey, measuring the temperature profile, and analyzing the sensitivity of the system parameters. The sites were located in Celukan Bawang and Bungkulan in North Bali, Indonesia. The comparison between the measured data and the HYCOM model data showed a good agreement, with the temperature difference between the surface and the 500-m deep cold water exceeding 20°C and meeting the temperature standards for OTEC systems.

Based on the calculation of Rankine Cycle OTEC systems, of the five types of working fluids (R290, R600a, R152a, R134a, and ammonia), the cycle with ammonia produced the highest net power output. However, in terms of cycle efficiency, the ammonia cycle was at the bottom of the list. In addition, using mass flow as an independent variable to adjust heat exchanger performance, it was shown that better heat exchanger performance (the lower  $\Delta T_{c,e}$ ) did not necessarily result in higher net power output and efficiency. Of the three variations used, the variation  $\Delta T_c = 3$  produced the highest net power and efficiency. In addition, the performance of the heat exchanger also greatly affected the seawater mass flowrate requirements of the system. Therefore, the diameter requirement of the seawater pipe increased with the increase in heat exchanger capacity.

## 6- Declarations

### 6-1-Author Contributions

Conceptualization, R.R., R.A., and T.Y.; methodology, R.A. and T.Y.; software, R.A.; validation, A.N., R.S., and W.P.; formal analysis, R.R. and R.A.; investigation, A.A., M.S., R.R., and R.A.; resources, R.R. and A.N.; data curation, R.A.; writing—original draft preparation, R.R. and R.A.; writing—review and editing, R.R. and R.A.; visualization, R.A.; supervision, A.N. and W.P.; project administration, M.S., R.R., and R.A.; funding acquisition, R.R., R.S., and A.N. All authors have read and agreed to the published version of the manuscript.

### 6-2-Data Availability Statement

The data presented in this study are available in the article.

### 6-3-Funding

The authors received financial support for the research and publication of this article from PT. PLN Research Institute.

#### 6-4-Acknowledgements

This work is part of the OTEC research activity “Pre-feasibility Study of OTEC Implementation in Indonesia,” conducted in a collaboration frame between the Ocean Energy Research Group (The Research Center for Hydrodynamics Technology, the National Research and Innovation Agency-BRIN), and the Power Generation System Research Department (PT PLN (Persero) Research Institute).

#### 6-5-Institutional Review Board Statement

Not applicable.

#### 6-6-Informed Consent Statement

Not applicable.

#### 6-7-Conflicts of Interest

The authors declare that there is no conflict of interest regarding the publication of this manuscript. In addition, the ethical issues, including plagiarism, informed consent, misconduct, data fabrication and/or falsification, double publication and/or submission, and redundancies have been completely observed by the authors.

### 7- References

- [1] Alanazi, M. A., Aloraini, M., Islam, M., Alyahya, S., & Khan, S. (2023). Wind Energy Assessment Using Weibull Distribution with Different Numerical Estimation Methods: A Case Study. *Emerging Science Journal*, 7(6), 2260-2278. doi:10.28991/ESJ-2023-07-06-024.
- [2] Wang, C. M., Yee, A. A., Krock, H., & Tay, Z. Y. (2011). Research and developments on ocean thermal energy conversion. *IES Journal Part A: Civil and Structural Engineering*, 4(1), 41–52. doi:10.1080/19373260.2011.543606.
- [3] Nihous, G. C., & Vega, L. A. (1993). Design of a 100 MW OTEC-hydrogen plantship. *Marine Structures*, 6(2–3), 207–221. doi:10.1016/0951-8339(93)90020-4.
- [4] Koto, J. (2016). Potential of Ocean Thermal Energy Conversion in Indonesia. *International Journal of Environmental Research & Clean Energy*, 4(1), 1–7.
- [5] Sinuhaji, A. R. (2015). Potential Ocean Thermal Energy Conversion (OTEC) in Bali. *KnE Energy*, 1(1), 5. doi:10.18502/ken.v1i1.330.
- [6] Adiputra, R., & Utsunomiya, T. (2018). Design Optimization of Floating Structure for a 100 MW-Net Ocean Thermal Energy Conversion (OTEC) Power Plant. Volume 10: *Ocean Renewable Energy*. doi:10.1115/omae2018-77539.
- [7] Adiputra, R., Utsunomiya, T., Koto, J., Yasunaga, T., & Ikegami, Y. (2020). Preliminary design of a 100 MW-net ocean thermal energy conversion (OTEC) power plant study case: Mentawai island, Indonesia. *Journal of Marine Science and Technology (Japan)*, 25(1), 48–68. doi:10.1007/s00773-019-00630-7.
- [8] Lutfi, Y. M., Adiputra, R., Prabowo, A. R., Utsunomiya, T., Erwandi, E., & Muhayat, N. (2023). Assessment of the stiffened panel performance in the OTEC seawater tank design: Parametric study and sensitivity analysis. *Theoretical and Applied Mechanics Letters*, 13(4). doi:10.1016/j.taml.2023.100452.
- [9] Adiputra, R., & Utsunomiya, T. (2019). Stability Analysis of Free Hanging Riser Conveying Fluid for Ocean Thermal Energy Conversion (OTEC) Utilization. Volume 9: *Rodney Eatock Taylor Honoring Symposium on Marine and Offshore Hydrodynamics; Takeshi Kinoshita Honoring Symposium on Offshore Technology*. doi:10.1115/omae2019-96749.
- [10] Adiputra, R., & Utsunomiya, T. (2019). Stability based approach to design cold-water pipe (CWP) for ocean thermal energy conversion (OTEC). *Applied Ocean Research*, 92. doi:10.1016/j.apor.2019.101921.
- [11] Adiputra, R., & Utsunomiya, T. (2021). Linear vs non-linear analysis on self-induced vibration of OTEC cold water pipe due to internal flow. *Applied Ocean Research*, 110. doi:10.1016/j.apor.2021.102610.
- [12] Adiputra, R., & Utsunomiya, T. (2022). Finite Element Modelling Of Ocean Thermal Energy Conversion (OTEC) Cold Water Pipe (CWP). *Proceedings of the International Conference on Offshore Mechanics and Arctic Engineering (OMAE)*. doi:10.1115/OMAE2022-78135.
- [13] Habib, M. I., Adiputra, R., Prabowo, A. R., Erwandi, E., Muhayat, N., Yasunaga, T., Ehlers, S., & Braun, M. (2023). Internal flow effects in OTEC cold water pipe: Finite element modelling in frequency and time domain approaches. *Ocean Engineering*, 288(116056). doi:10.1016/j.oceaneng.2023.116056.
- [14] Adie, P. W., Prabowo, A. R., Muttaqie, T., Adiputra, R., Muhayat, N., Carvalho, H., & Huda, N. (2023). Non-linear assessment of cold water pipe (CWP) on the ocean thermal energy conversion (OTEC) installation under bending load. *Procedia Structural Integrity*, 47, 142–149. doi:10.1016/j.prostr.2023.07.005.

- [15] Adie, P. W., Adiputra, R., Prabowo, A. R., Erwandi, E., Muttaqie, T., Muhayat, N., & Huda, N. (2023). Assessment of the OTEC cold water pipe design under bending loading: A benchmarking and parametric study using finite element approach. *Journal of the Mechanical Behavior of Materials*, 32(1). doi:10.1515/jmbm-2022-0298.
- [16] McCallister, M., Switzer, T., Arnold, F., & Ericksen, T. (2010). Geophysical and oceanographic site survey requirements for Ocean Thermal Energy Conversion (OTEC) installations. *OCEANS 2010 MTS/IEEE*, Seattle, United States. doi:10.1109/oceans.2010.5664488.
- [17] Abraham, J. P., Baringer, M., Bindoff, N. L., Boyer, T., Cheng, L. J., Church, J. A., Conroy, J. L., Domingues, C. M., Fasullo, J. T., Gilson, J., Goni, G., Good, S. A., Gorman, J. M., Gouretski, V., Ishii, M., Johnson, G. C., Kizu, S., Lyman, J. M., Macdonald, A. M., ... Willis, J. K. (2013). A review of global ocean temperature observations: Implications for ocean heat content estimates and climate change. *Reviews of Geophysics*, 51(3), 450–483. doi:10.1002/rog.20022.
- [18] Samsuri, N., Shaikh Salim, S. A. Z., Musa, M. N., & Mat Ali, M. S. (2016). Modelling Performance Of Ocean-Thermal Energy Conversion Cycle According To Different Working Fluids. *Jurnal Teknologi*, 78(11). doi:10.11113/v78.8741.
- [19] Liu, W., Xu, X., Chen, F., Liu, Y., Li, S., Liu, L., & Chen, Y. (2020). A review of research on the closed thermodynamic cycles of ocean thermal energy conversion. *Renewable and Sustainable Energy Reviews*, 119. doi:10.1016/j.rser.2019.109581.
- [20] Avery, W. H., & Wu, C. (1994). *Renewable energy from the ocean: a guide to OTEC*. Oxford university press, Oxford, United Kingdom. doi:10.1016/0029-8018(95)90035-7.
- [21] Eldred, M. P., Van Ryzin, J. C., Rizea, S., Chen, I. C., Loudon, R., Nagurny, N. J., Maurer, S., Jansen, E., Plumb, A., Eller, M. R., & Brown, V. R. R. (2011). Heat exchanger development for Ocean Thermal Energy Conversion. *OCEANS'11 MTS/IEEE KONA*, Waikoloa, United States. doi:10.23919/oceans.2011.6107175.
- [22] Fontaine, K., Yasunaga, T., & Ikegami, Y. (2019). OTEC maximum net power output using carnot cycle and application to simplify heat exchanger selection. *Entropy*, 21(12). doi:10.3390/e21121143.
- [23] Thirugnana, S. T., Jaafar, A. B., Rajoo, S., Azmi, A. A., Karthikeyan, H. J., Yasunaga, T., Nakaoka, T., Kamyab, H., Chelliapan, S., & Ikegami, Y. (2023). Performance Analysis of a 10 MW Ocean Thermal Energy Conversion Plant Using Rankine Cycle in Malaysia. *Sustainability (Switzerland)*, 15(4), 3777. doi:10.3390/su15043777.
- [24] Langer, J., Cahyaningwidi, A. A., Chalkiadakis, C., Quist, J., Hoes, O., & Blok, K. (2021). Plant siting and economic potential of ocean thermal energy conversion in Indonesia a novel GIS-based methodology. *Energy*, 224, 224. doi:10.1016/j.energy.2021.120121.
- [25] Samsuri, N., Sazali, N., Jamaludin, A. S., & Razali, M. N. M. (2021). Techno-economic efficiencies and environmental criteria of Ocean Thermal Energy Conversion closed Rankine cycle using different working fluids. *IOP Conference Series: Materials Science and Engineering*, 1062(1), 012042. doi:10.1088/1757-899X/1062/1/012042.
- [26] Lee, B., Wang, Z., & Gong, N. (2022). A Study on Performance of Rankine Cycle Used in OTEC Power Plant. *SSRN Electronic Journal*. doi:10.2139/ssrn.4112974.
- [27] Nakaoka, T., & Uehara, H. (1988). Performance test of a shell-and-plate type evaporator for OTEC. *Experimental Thermal and Fluid Science*, 1(3), 283–291. doi:10.1016/0894-1777(88)90008-8.
- [28] Syamsuddin, M. L., Attamimi, A., Nugraha, A. P., Gibran, S., Afifah, A. Q., & Oriana, N. (2015). OTEC Potential in the Indonesian Seas. *Energy Procedia*, 65, 215–222. doi:10.1016/j.egypro.2015.01.028.
- [29] Yang, M. H., & Yeh, R. H. (2014). Analysis of optimization in an OTEC plant using organic Rankine cycle. *Renewable Energy*, 68, 25–34. doi:10.1016/j.renene.2014.01.029.
- [30] Ikegami, Y., Yasunaga, T., & Morisaki, T. (2018). Ocean Thermal Energy Conversion using double-stage Rankine Cycle. *Journal of Marine Science and Engineering*, 6(1). doi:10.3390/jmse6010021.
- [31] Dijoux, A., Sinama, F., Marc, O., & Castaing-Lasvignottes, J. (2019). Modelling and experimentation of heat exchangers for Ocean Thermal Energy Conversion during transient operation. *Procedia Manufacturing*, 35, 298–303. doi:10.1016/j.promfg.2019.05.043.
- [32] Sinama, F., Martins, M., Journoud, A., Marc, O., & Lucas, F. (2015). Thermodynamic analysis and optimization of a 10MW OTEC Rankine cycle in Reunion Island with the equivalent Gibbs system method and generic optimization program GenOpt. *Applied Ocean Research*, 53, 54–66. doi:10.1016/j.apor.2015.07.006.
- [33] Yasunaga, T., Fontaine, K., Morisaki, T., & Ikegami, Y. (2017). Performance evaluation of heat exchangers for application to ocean thermal energy conversion system. *Performance Evaluation of Heat Exchangers for Application to Ocean Thermal Energy Conversion System*, 22, 65–75.
- [34] Alrwashdeh, S. S., Ammari, H., Madanat, M. A., & Al-Falahat, A. M. (2022). The Effect of Heat Exchanger Design on Heat transfer Rate and Temperature Distribution. *Emerging Science Journal*, 6(1), 128–137. doi:10.28991/ESJ-2022-06-01-010.



- [35] Yeh, R. H., Su, T. Z., & Yang, M. S. (2005). Maximum output of an OTEC power plant. *Ocean Engineering*, 32(5–6), 685–700. doi:10.1016/j.oceaneng.2004.08.011.
- [36] Hernández-Romero, I. M., Nápoles-Rivera, F., Flores-Tlacuahuac, A., & Fuentes-Cortés, L. F. (2020). Optimal design of the ocean thermal energy conversion systems involving weather and energy demand variations. *Chemical Engineering and Processing - Process Intensification*, 157. doi:10.1016/j.cep.2020.108114.
- [37] Herrera, J., Sierra, S., Hernández-Hamón, H., Ardila, N., Franco-Herrera, A., & Ibeas, A. (2022). Economic Viability Analysis for an OTEC Power Plant at San Andrés Island. *Journal of Marine Science and Engineering*, 10(6). doi:10.3390/jmse10060713.
- [38] Ganic, E. N., & Wu, J. (1979). Comparative study of working fluids for OTEC power plants (No. ANL/OTEC-TM-1). Department of Energy Engineering, University of Chicago, Chicago, United States.
- [39] Hung, T. C., Wang, S. K., Kuo, C. H., Pei, B. S., & Tsai, K. F. (2010). A study of organic working fluids on system efficiency of an ORC using low-grade energy sources. *Energy*, 35(3), 1403–1411. doi:10.1016/j.energy.2009.11.025.
- [40] Sun, F., Ikegami, Y., Jia, B., & Arima, H. (2012). Optimization design and exergy analysis of organic rankine cycle in ocean thermal energy conversion. *Applied Ocean Research*, 35, 38–46. doi:10.1016/j.apor.2011.12.006.
- [41] Sazonov, Y. A., Mokhov, M. A., Gryaznova, I. V., Voronova, V. V., Tumanyan, K. A., & Konyushkov, E. I. (2023). Thrust Vector Control within a Geometric Sphere, and the Use of Euler's Tips to Create Jet Technology. *Civil Engineering Journal*, 9(10), 2516-2534. doi:10.28991/CEJ-2023-09-10-011.
- [42] Yang, M. H., & Yeh, R. H. (2014). Analysis of optimization in an OTEC plant using organic Rankine cycle. *Renewable Energy*, 68, 25–34. doi:10.1016/j.renene.2014.01.029.